

## Global phase diagram for the honeycomb potential

Antti-Pekka Hynninen and Athanassios Z. Panagiotopoulos

*Department of Chemical Engineering, Princeton University, Princeton, New Jersey 08544 and Princeton Institute for the Science and Technology of Materials, Princeton University, Princeton, New Jersey 08544*

Mikael C. Rechtsman

*Department of Physics, Princeton University, Princeton, New Jersey 08544*

Frank H. Stillinger

*Department of Chemistry, Princeton University, Princeton, New Jersey 08544*

Salvatore Torquato<sup>a)</sup>

*Department of Chemistry, Princeton University, Princeton, New Jersey 08544; Program in Applied and Computational Mathematics, Princeton University, Princeton, New Jersey 08544; Princeton Institute for the Science and Technology of Materials, Princeton University, Princeton, New Jersey 08544; and Princeton Center for Theoretical Physics, Princeton University, Princeton, New Jersey 08544*

(Received 8 May 2006; accepted 22 May 2006; published online 13 July 2006)

We calculate the global phase diagram using classical statistical mechanics for an isotropic pair potential that has been previously [Rechtsman *et al.*, *Phys. Rev. Lett.* **95**, 228301 (2005)] shown to produce the low-coordinated two-dimensional honeycomb crystal as the ground-state structure. Low-coordinated crystals are of practical interest because they have desirable photonic band-gap properties. The phase diagram is obtained from Helmholtz free energies calculated using thermodynamic integration and Monte Carlo simulations. Our results show that the honeycomb crystal remains stable in the global phase diagram even after temperature effects are taken fully into account. Other stable phases in the phase diagram are high and low density triangular phases and a fluid phase. We find no evidence of gas-liquid or liquid-liquid phase coexistence. © 2006 American Institute of Physics. [DOI: [10.1063/1.2213611](https://doi.org/10.1063/1.2213611)]

### I. INTRODUCTION

Self-assembly is the process whereby components of a system arrange themselves into a larger functional unit by virtue of their mutual interactions.<sup>1</sup> It is a truly ubiquitous phenomenon in nature. The spontaneous folding of a protein into its native state, the formation of the DNA double helix from two complementary oligonucleotide chains, and the formation of lipid bilayers as membranes are just a few biological examples. Synthetic self-assembling systems, especially on the nanoscale, have been the focus of much research in the last decade, as their technological importance has become more and more apparent. Examples of these are block copolymer nanostructures,<sup>2</sup> colloidal and nanoparticle crystals,<sup>3</sup> and organometallic patterning in two dimensions.<sup>4</sup> A particularly ambitious goal is the self-assembly of the diamond lattice colloidal crystal, which has been called the “holy grail” of colloid science, since such a material has a full photonic bandgap and could thus be used in photonic circuitry. As we reach the limits of resolution of conventional microlithography, self-assembly is becoming widely viewed as the best method of engineering extended nanoscale structures, and hence, the key materials of the future.

Attempts to find systems that will self-assemble into desired structures have been largely based on trial and error rather than on any systematic procedure. Despite much ex-

perimental and theoretical research that has been carried out in the search for exotic and technologically relevant self-assembling systems, there has been no accepted theoretical framework for the process of self-assembly as a whole. In a preceding study by some of us,<sup>5,6</sup> a statistical-mechanical inverse method was formulated that allows one to optimize interactions that stabilize a target crystalline, amorphous, or even quasicrystalline structure. The optimization method was applied in two dimensions to produce isotropic pair potentials that give rise to the low-coordinated square and honeycomb crystals. In Refs. 5 and 6, the stability of the crystal structures was based on lattice sums, mechanical stability (phonon spectra), and annealed Monte Carlo (MC) simulations. While these methods guarantee stability, they do not give information on the global phase behavior where the effects due to temperature (or, equivalently, entropy) are included. Moreover, the knowledge of the global phase behavior is of importance for experimental colloidal studies that seek to achieve the target crystal structures.

Motivated by these recent studies,<sup>5,6</sup> in the current paper we examine the global phase behavior of what we call a “honeycomb potential,” i.e., the interaction potential that in Refs. 5 and 6 was shown to stabilize the honeycomb crystal. We use classical statistical mechanics and the phase diagram is obtained from Helmholtz free energies calculated using thermodynamic integration and Monte Carlo simulations. We find that the honeycomb crystal is indeed stable in the global phase diagram along with two triangular phases and a fluid

<sup>a)</sup>Electronic mail: [torquato@electron.princeton.edu](mailto:torquato@electron.princeton.edu)

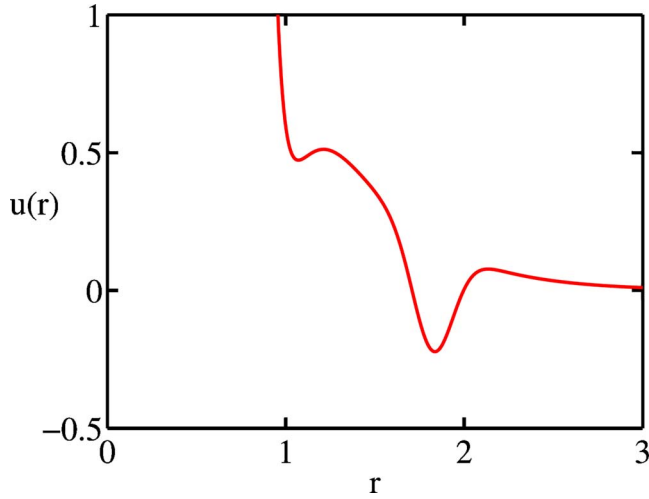


FIG. 1. The honeycomb potential.

phase. We also find that the phase diagram is dominated by fluid-solid and solid-solid phase coexistence regions, and we find no evidence of gas-liquid or liquid-liquid phase separation.

This paper is organized as follows. In Sec. II, we describe the methods used to calculate the phase diagram. In Sec. III, we discuss the results, including the phase diagram and snapshots of the system. We close with concluding remarks and related discussion in Sec. IV.

## II. METHODS

The so-called honeycomb pair potential  $u(r)$  used in this paper is given by<sup>5,6</sup>

$$u(r) = \frac{5}{r^{12}} - \frac{5.89}{r^{10}} + 17.9 \exp(-2.49r) - 0.4 \exp[-40(r - 1.823)^2] \quad (1)$$

and is plotted in Fig. 1. In Eq. (1), the potential  $u(r)$  and the radial distance  $r$  are expressed in reduced units of energy ( $\epsilon$ ) and distance ( $\sigma$ ), respectively. We can then define the reduced temperature as  $T = k_B T' / \epsilon$  and the reduced (spreading) pressure as  $P = P' \sigma^3 / k_B T'$ , where  $T'$  and  $P'$  are the conventional temperature and pressure, respectively. The pair potential has two minima: a shallow one at  $r \approx 1.07$  and a slightly deeper one at  $r \approx 1.84$ . In Refs. 5 and 6 this potential was shown to give rise to the self-assembly of the honeycomb crystal. We point out that our potential in Eq. (1) is similar in form to the Stell-Hemmer core-softened potential,<sup>7-10</sup> which has been studied in two dimensions in Refs. 11 and 12.

The Helmholtz free energy of the solid phases was calculated using the Frenkel-Ladd method.<sup>13,14</sup> In this method, one starts from an Einstein crystal where the particles are tied to their ideal lattice positions by harmonic springs. Then, the springs are slowly removed and one recovers the original interactions. The auxiliary potential energy function for  $N$  particles at  $\mathbf{r}^N = \{\mathbf{r}_{ij}\}_{i=1}^N$  is given by

$$U_\lambda(\mathbf{r}^N) = U(\mathbf{r}^N) + T\lambda\alpha \sum_{i=1}^N (\mathbf{r}_i - \mathbf{r}_{0,i})^2, \quad (2)$$

where  $U(\mathbf{r}^N) = \sum_{i<j}^N u(|\mathbf{r}_i - \mathbf{r}_j|)$  is the total potential energy,  $\mathbf{r}_{0,i}$  is the ideal lattice position of particle  $i$ ,  $\alpha$  is a dimensionless spring constant, and  $\lambda \in [0, 1]$  is a coupling parameter. At  $\lambda=0$ , we recover the system where particles interact via the honeycomb potential, while at  $\lambda=1$ , once the spring constant  $\alpha$  is chosen large enough (we used  $\alpha = 8 \times 10^4$ ), the particles do not “feel” each other and the system reduces to an Einstein crystal with Madelung energy  $U(\mathbf{r}_0^N)$  (the potential energy of a crystal with all particles at their ideal lattice positions). The Helmholtz free energy for a system of  $N$  particles on area  $A$  at temperature  $T$  is given by<sup>13-15</sup>

$$F(N, A, T) = F_{\lambda=1}(N, A, T, \alpha) - T \int_0^1 d\lambda \left\langle \alpha \sum_{i=1}^N (\mathbf{r}_i - \mathbf{r}_{0,i})^2 \right\rangle_\lambda^{\text{CM}}, \quad (3)$$

where the ensemble average  $\langle \dots \rangle_\lambda^{\text{CM}}$  is calculated with a Boltzmann factor  $\exp(-U_\lambda/T)$  for a crystal with a fixed center of mass (CM), and the free energy of the reference state is given by

$$F_{\lambda=1}(N, A, T, \alpha) = U(\mathbf{r}_0^N) + (N-1)T \ln\left(\frac{\alpha}{\pi}\right) - T \ln(A). \quad (4)$$

In practice, the integral in Eq. (3) was calculated using the Gauss-Legendre quadrature<sup>16</sup> with ten integration points. In order to obtain a more slowly varying function for the numerical integration, we changed the integration variable  $\lambda$  to  $\ln(\lambda\alpha + c)$ , where  $c = 1 / \langle \sum_{i=1}^N (\mathbf{r}_i - \mathbf{r}_{0,i})^2 \rangle_0^{\text{CM}}$ , see Ref. 13.

The Helmholtz free energy of a fluid phase was calculated using the Kirkwood’s coupling parameter method,<sup>13,17</sup> where we used the two-dimensional Weeks-Chandler-Anderson<sup>18</sup> (WCA) fluid as the reference state. The auxiliary potential energy function is given by

$$U_\xi(\mathbf{r}^N) = (1 - \xi)U_{\text{WCA}}(\mathbf{r}^N) + \xi U(\mathbf{r}^N), \quad (5)$$

where  $U_{\text{WCA}}(\mathbf{r}^N) = \sum_{i<j}^N u_{\text{WCA}}(|\mathbf{r}_i - \mathbf{r}_j|)$  is the total potential energy of a WCA fluid,  $\xi \in [0, 1]$ , and

$$u_{\text{WCA}}(r) = \begin{cases} 4[(1/r)^{12} - (1/r)^6 + 1/4] & \text{for } r < 2^{1/6} \\ 0 & \text{for } r \geq 2^{1/6}. \end{cases} \quad (6)$$

The Helmholtz free energy is given by

$$F(N, A, T) = F_{\text{WCA}}(N, A, T) + \int_0^1 \langle U(\mathbf{r}^N) - U_{\text{WCA}}(\mathbf{r}^N) \rangle_\xi d\xi, \quad (7)$$

where  $F_{\text{WCA}}(N, A, T)$  is the free energy of a two-dimensional WCA fluid. We calculated  $F_{\text{WCA}}(N, A, T)$  from the numerical integration of the scaled particle theory<sup>19</sup> equation of state given by

$$\frac{P(\rho, T)}{\rho} = \frac{1}{[1 - (\pi/4)\rho d(T)^2]^2}, \quad (8)$$

where  $\rho = N/A$  is the number density, and

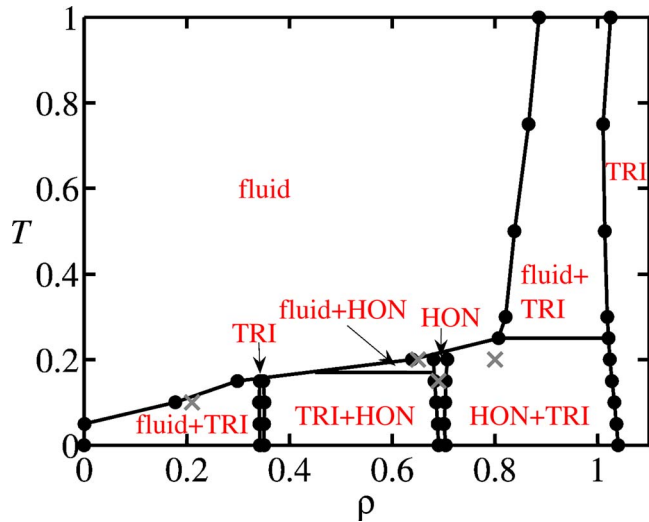


FIG. 2. The phase diagram for the honeycomb potential in the reduced density  $\rho$ , reduced temperature  $T$  representation. The black circles denote the points where two phases coexist. The statistical uncertainties are smaller than the symbol sizes. The regions of stable fluid, triangular, and honeycomb phases are indicated by the labels “fluid,” “TRI,” and “HON,” respectively, and the coexistence regions are marked by “fluid+TRI,” “TRI+HON,” etc., and the tie lines are horizontal. The black lines are guide to the eye, and the crosses indicate the locations where the snapshots in Figs. 4–7 are taken.

$$d(T) = \frac{0.3837T + 1.068}{0.4293T + 1} \quad (9)$$

is the effective diameter according to Verlet and Weis.<sup>20</sup> This combination of the equation of state and the effective diameter has been shown to give good agreement with computer simulations at all densities and temperatures.<sup>21</sup> The integral in Eq. (7) was calculated using the Gauss-Legendre quadrature<sup>16</sup> with ten integration points.

The number of particles used in the free energy calculations was 264 for the triangular and fluid phases, and 270 for the honeycomb phase. These particle numbers are commensurate with the triangular and honeycomb lattice structures and produce nearly square shaped simulation boxes. In the fluid phase simulations, the box was always square shaped. We used the standard Metropolis Monte Carlo method<sup>22</sup> and applied periodic boundary conditions in both coordinate directions. The interaction potential in Eq. (1) was truncated at half of the smaller simulation box side length. This results in a relative cutoff error in the total energy per particle of order  $10^{-5}$  or less, which is negligible compared to the statistical error in the average total energy per particle that is of order  $10^{-3}$ . The ensemble averages were obtained from MC simulations that consisted of  $10^4$  equilibration steps (trials to displace each particle once) and  $2 \times 10^4$  sampling steps. Additionally, we performed constant pressure simulations and calculated the equation of state at various temperatures. The constant pressure MC runs consisted of  $10^5$  equilibration steps and  $2 \times 10^5$  sampling steps, and they were used both to check the phase diagram for presence of crystals other than the triangular and honeycomb, and to test the fluid phase free energy data.

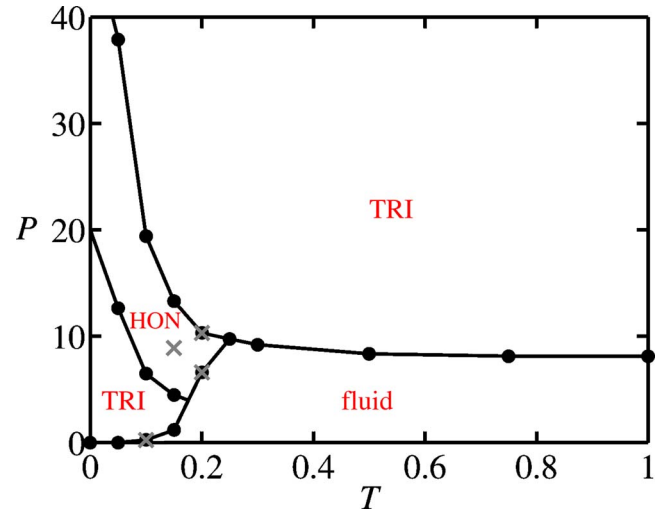


FIG. 3. The phase diagram for the honeycomb potential in the reduced temperature  $T$ , reduced pressure  $P$  representation. The regions of stable fluid, triangular, and honeycomb phases are indicated by the labels fluid, TRI, and HON respectively. The black circles denote the points where two phases coexist. The statistical uncertainties are smaller than the symbol sizes. The black lines are guide to the eye, and the crosses indicate the locations where the snapshots in Figs. 4–7 are taken.

### III. RESULTS AND DISCUSSION

The phase diagram for the honeycomb potential is shown in the reduced density  $\rho$ , reduced temperature  $T$  representation in Fig. 2, and in the reduced temperature  $T$ , reduced pressure  $P$  representation in Fig. 3. In Figs. 2 and 3, the regions of stable fluid, triangular, and honeycomb phases are indicated by the labels “fluid,” “TRI,” and “HON,” respectively. In Fig. 2, the two-phase coexistence regions are labeled as “fluid+TRI,” “TRI+HON,” etc. As can be seen from Figs. 2 and 3, at low temperatures and with increasing density or pressure, the sequence of phases is fluid, triangular, honeycomb, and triangular. There are therefore two triangular phases, one at low density and one at high density. The sequence triangular-honeycomb-triangular can be understood based on the following reasoning. In the low density triangular phase at density  $\rho=0.34$ , the nearest-neighbor distance is approximately 1.84, which corresponds to the location of the deeper minimum in the interaction potential at  $r \approx 1.84$ . As the density is increased to  $\rho=0.69$ , the honeycomb crystal becomes stable because it has the nearest neighbors at distance  $r \approx 1.06$ , close to the shallow minimum at  $r \approx 1.07$ , and the next nearest neighbors at distance  $r \approx 1.83$ , close to the deeper minimum at  $r \approx 1.84$ . At density  $\rho=1.02$ , the triangular phase is again stable because it has the nearest-neighbor distance of  $r \approx 1.06$  that is close to the shallow minimum at  $r \approx 1.07$ . At ever higher  $\rho$ , the triangular lattice remains stable as the strongly repulsive core region of  $u(r)$  dominates nearest-neighbor interactions.

As is seen from Fig. 2, the regions of stable triangular and honeycomb crystals are small compared to the surrounding fluid-triangular and triangular-honeycomb coexistence regions. We also observe that the density of the stable triangular and honeycomb phases remains approximately constant with increasing temperature. The low density triangular phase terminates at a triple point at  $T \approx 0.17$ , and the honey-

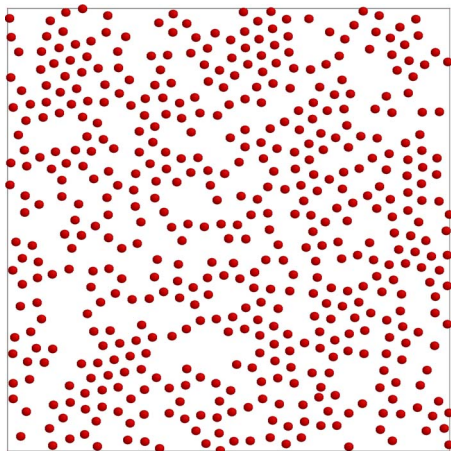


FIG. 4. Snapshot of a system with  $N=500$  particles at  $T=0.1$  and  $\rho=0.21$ , where fluid is in coexistence with a low density triangular crystal.

comb phase terminates at a triple point at  $T \approx 0.21$ . Note that both triple points are only rough estimates and that more free energy calculations would be needed to determine them more accurately. At  $T \geq 0.25$ , the only stable phases are the fluid phase and the high density triangular phase. At higher temperatures still, the system is dominated by the repulsive core of  $u(r)$ , and one thus obtains the familiar fluid-triangular phase coexistence similar to hard disks.<sup>23</sup> According to the Kosterlitz-Thoules-Halperin-Nelson-Young (KTHNY) theory,<sup>24–28</sup> in two-dimensional systems like ours, it is expected that solid phases melt via two continuous transitions. Since studies of the KTHNY transition require somewhat larger system sizes than the ones used in the present study, and because we expect the hexatic phase predicted by the KTHNY theory to play a negligible role in the phase diagram, we have chosen not to look for the two-stage melting here.

It is interesting to note that the phase diagram does not contain a gas-liquid phase coexistence region in the low temperature, low density part of the phase diagram. Instead, this part of the phase diagram is dominated by a broad gas-solid coexistence. Such behavior has been previously observed for interaction potentials that have a narrow potential well

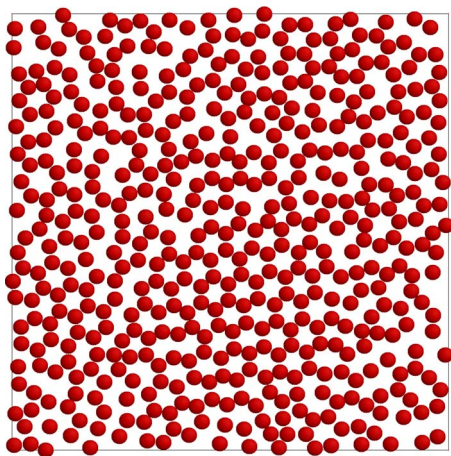


FIG. 5. Snapshot of a system with  $N=500$  particles at  $T=0.2$  and  $\rho=0.65$ , where fluid is in coexistence with a honeycomb crystal.

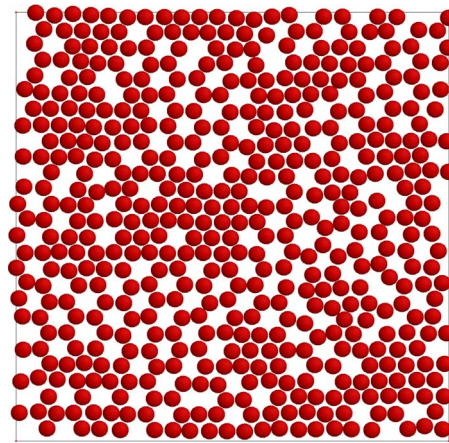


FIG. 6. Snapshot of a system with  $N=505$  particles at  $T=0.2$  and  $\rho=0.8$ , where a honeycomb crystal is in coexistence with a high density triangular crystal.

minimum,<sup>29,30</sup> such as the one used in this study. We also find no evidence of liquid-liquid phase coexistence, although conceivably this could be present because the potential has two minima.

The statistical uncertainties in Figs. 2 and 3 are smaller than the symbol sizes. The systematic error due to finite system size was studied by repeating the calculations at approximately half as many particles. Halving the system size shifted the fluid side of the fluid-triangular coexistence line at the high density, high temperature ( $T \geq 0.25$ ) part of the phase diagram to higher densities by less than 0.1, while other parts of the phase diagram changed by less than the symbol size. Since doubling the system size did not change the high density, high temperature part of the phase diagram, we conclude that the systematic error due to finite system size is unlikely to change the main features of the phase diagram.

Figures 4–7 show snapshots of systems at certain points in the phase diagram. The locations of the snapshots in Figs. 4–7 are indicated in Figs. 2 and 3 by the gray crosses. The snapshot in Fig. 4 is taken at  $T=0.1$  and  $\rho=0.21$ , where fluid is in coexistence with a low density triangular crystal. In Fig. 4, one sees small areas of crystal order surrounded by a fluid that is rather structured and consists of voids and particles

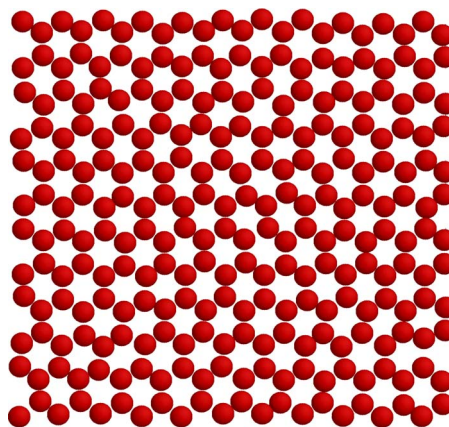


FIG. 7. Snapshot of stable honeycomb crystal with  $N=264$  particles at  $T=0.15$  and  $\rho=0.69$ .

that are mostly distance  $r \approx 1.84$  apart from each other. The snapshot in Fig. 5 is taken at  $T=0.2$  and  $\rho=0.65$ , where fluid is in coexistence with a honeycomb crystal. The snapshot in Fig. 6 is taken at  $T=0.2$  and  $\rho=0.8$ , where a honeycomb crystal is in coexistence with a high density triangular crystal. The snapshot in Fig. 7 shows stable honeycomb crystal at  $T=0.15$  and  $\rho=0.69$ .

#### IV. CONCLUSIONS

We have calculated the global phase diagram for an isotropic pair potential that has been designed to give the low-coordinated two-dimensional honeycomb crystal.<sup>5,6</sup> Our results show that the honeycomb crystal is indeed stable in the global phase diagram at positive temperatures. In the low temperature region, we find a sequence of fluid, triangular, honeycomb, and triangular phases connected by two-phase coexistence regions. We did not find evidence of a gas-liquid or liquid-liquid phase coexistence but instead found a gas-solid phase coexistence.

In the density-temperature representation, the size of the coexistence regions is much larger than the size of stable region of the honeycomb crystal. This is so because the search algorithm that was used to find the interaction potential was designed to optimize the potential close to the  $T=0$  limit. Large coexistence regions could mean difficulties for experimental studies that try to realize the honeycomb crystal, especially if the interaction potential is density dependent. Since the size of the stable region of the honeycomb crystal is larger in the pressure-temperature representation, a tactically better way to achieve the honeycomb crystal would be to perform the experiments at constant spreading pressure instead of constant density. It would also be interesting to see if one would be able to establish a statistical-mechanical inverse method that searches for interaction potentials that give rise to large single-phase regions instead of two-phase coexistence. Such methods would have to include, in addition to the lattice sums, an estimate of the entropic contribution to the free energy.

#### ACKNOWLEDGMENTS

This work was partially supported by the NSF (MRSEC Program) through the Princeton Center for Complex Materi-

als (DMR 0213706) through a PCCM Fellowship to one of the authors (A.P.H.). Additional support was provided by ACS-PRF (Grant No. 38165-AC9) to another author (A.Z.P.). Three of the authors (M.C.R., F.H.S., and S.T.) gratefully acknowledge the support by the Office of Basic Energy Sciences, DOE, under Grant No. DE-FG02-04ER46108.

- <sup>1</sup>G. M. Whitesides and B. Grzybowski, *Science* **295**, 2418 (2002).
- <sup>2</sup>S. A. Jenekhe and X. L. Chen, *Science* **283**, 372 (1999).
- <sup>3</sup>Z. Cheng, W. B. Russel, and P. M. Chaikin, *Nature (London)* **401**, 893 (1999).
- <sup>4</sup>G. M. Whitesides and P. E. Laibinis, *Langmuir* **6**, 87 (1990).
- <sup>5</sup>M. C. Rechtsman, F. H. Stillinger, and S. Torquato, *Phys. Rev. Lett.* **95**, 228301 (2005).
- <sup>6</sup>M. C. Rechtsman, F. H. Stillinger, and S. Torquato, *Phys. Rev. E* **73**, 011406 (2006).
- <sup>7</sup>P. C. Hemmer and G. Stell, *Phys. Rev. Lett.* **24**, 1284 (1970).
- <sup>8</sup>G. Stell and P. C. Hemmer, *J. Chem. Phys.* **56**, 4274 (1972).
- <sup>9</sup>J. M. Kincaid, G. Stell, and C. K. Hall, *J. Chem. Phys.* **65**, 2161 (1976).
- <sup>10</sup>J. M. Kincaid, G. Stell, and E. Goldmark, *J. Chem. Phys.* **65**, 2172 (1976).
- <sup>11</sup>M. R. Sadr-Lahijany, A. Scala, S. V. Buldyrev, and H. E. Stanley, *Phys. Rev. Lett.* **81**, 4895 (1998).
- <sup>12</sup>N. B. Wilding and J. E. Magee, *Phys. Rev. E* **66**, 031509 (2002).
- <sup>13</sup>D. Frenkel and B. Smit, *Understanding Molecular Simulations*, 2nd ed. (Academic, New York, 2002).
- <sup>14</sup>D. Frenkel and A. J. C. Ladd, *J. Chem. Phys.* **81**, 3188 (1984).
- <sup>15</sup>J. M. Polson, E. Trizac, S. Pronk, and D. Frenkel, *J. Chem. Phys.* **112**, 5339 (2000).
- <sup>16</sup>M. Abramowitz and I. Stegun, *Handbook of Mathematical Functions* (Dover, New York, 1970).
- <sup>17</sup>J. G. Kirkwood, *J. Chem. Phys.* **3**, 300 (1935).
- <sup>18</sup>J. D. Weeks, D. Chandler, and H. C. Andersen, *J. Chem. Phys.* **54**, 5237 (1971).
- <sup>19</sup>E. Helfand, H. L. Frisch, and J. L. Lebowitz, *J. Chem. Phys.* **34**, 1037 (1961).
- <sup>20</sup>L. Verlet and J. J. Weis, *Mol. Phys.* **24**, 1013 (1972); *Phys. Rev. A* **5**, 939 (1972).
- <sup>21</sup>F. Cuadros and A. Mulero, *Chem. Phys.* **156**, 33 (1991).
- <sup>22</sup>N. Metropolis, A. W. Rosenbluth, M. N. Rosenbluth, A. H. Teller, and E. Teller, *J. Chem. Phys.* **21**, 1087 (1953).
- <sup>23</sup>B. J. Alder and T. E. Wainwright, *Phys. Rev.* **127**, 359 (1962).
- <sup>24</sup>J. M. Kosterlitz and D. J. Thouless, *J. Phys. C* **6**, 1181 (1973).
- <sup>25</sup>J. M. Kosterlitz, *J. Phys. C* **7**, 1046 (1974).
- <sup>26</sup>B. I. Halperin and D. R. Nelson, *Phys. Rev. Lett.* **41**, 121 (1978).
- <sup>27</sup>D. R. Nelson and B. I. Halperin, *Phys. Rev. B* **19**, 2457 (1979).
- <sup>28</sup>A. P. Young, *Phys. Rev. B* **19**, 1855 (1979).
- <sup>29</sup>A. P. Gast, C. K. Hall, and W. B. Russel, *J. Colloid Interface Sci.* **96**, 251 (1983).
- <sup>30</sup>M. H. J. Hagen and D. Frenkel, *J. Chem. Phys.* **101**, 4093 (1994).